



FREQUENCY WAVENUMBER AND SPATIAL AUTOCORRELATION METHODS FOR DISPERSION CURVE DETERMINATION FROM AMBIENT VIBRATION RECORDINGS

**Matthias OHRNBERGER¹, Estelle SCHISSELE², Cecile CORNOU³,
Sylvette BONNEFOY-CLAUDET⁴, Marc WATHELET⁵,
Alexandros SAVVAIDIS⁶, Frank SCHERBAUM⁷, Denis JONGMANS⁸**

SUMMARY

Analyzing simulated ambient vibrations we compared the reliability of several frequency-wavenumber array techniques and the spatial autocorrelation method for the estimation of dispersion curves (DC). We evaluated the influence of array configuration, source distribution and propagation effects on the DC-estimation. All f-k methods perform reasonably well, but a reliable interpretation of dispersion curves is limited to a restricted frequency band. In comparison, the spatial autocorrelation method shows a great sensitivity to the dispersion characteristics for a larger frequency range. We suggest to use a combination of methods for both determination of the valid frequency range and to obtain uncertainty limits.

INTRODUCTION

The influence of local surface geology on earthquake ground motion, generally termed site effect, is a well established concept developed during the last decades (Borcherdt [1], Campbell [2]). The quantitative assessment of site effects is therefore a major issue in seismic hazard and engineering seismology studies. Frequency dependent site amplifications are known to be mainly caused by reverberations and resonance effects of S-waves within unconsolidated sediments overlaying stiffer formations. Thus, it is of key interest to determine the shallow shear wave velocity structure (Hartzell et al. [3], Yamanaka [4]). In recent years, the analysis of ambient seismic vibrations has gained considerable attention for retrieving the subsurface shear velocity structure. Based on the notion that ambient vibrations are composed mainly of surface waves, shear wave velocity profiles down to depths of several hundred meters have been determined by inversion of dispersion curves obtained from ambient vibration array recordings (Horike [5], Ishida et al. [6], Miyakoshi et al. [7], Yamanaka et al. [8], Scherbaum et al. [9]). The major advantages of the ambient vibration technique are the low cost exploration and

¹Inst. f. Geowissenschaften, Universität Potsdam, Potsdam, Germany

²Inst. f. Geowissenschaften, Universität Potsdam, Potsdam, Germany

³Schweizer Erdbebendienst (SED), ETHZ, Zürich, Switzerland

⁴LGIT, Université Joseph Fourier, Grenoble, France

⁵GEOMAC, Université de Liege, Liege, Belgium

⁶Inst. of Eng. Seismology & Earthquake Eng. (ITSAK), Thessaloniki, Greece

⁷Inst f. Geowissenschaften, Universität Potsdam, Potsdam, Germany

⁸LIRIGM, Grenoble, France

monitoring capabilities, the possibility to perform non-destructive measurements at every place of a densely populated city, and the relatively large penetration depth.

The use of array methods for microtremor analysis started with Aki's [10] pioneering work. Aki demonstrated that, by analyzing the spatial correlation of ambient seismic noise recordings, small aperture arrays could be used to measure phase velocities of surface waves. From these dispersion characteristics, S-wave velocity profiles may then be derived by inversion. In the 1960's frequency-wavenumber (f-k) methods were applied to investigate the properties of the ambient noise wavefield (e.g. Lacoss et al. [11]). Further work (Horike [5],[12]; Matsushima and Okada [13]) coupled the SPAC method with high-resolution f-k (frequency-wavenumber) analysis (Capon [14]). Until today, several studies worldwide illustrate the practical interest in these techniques which may favorably compete with other methods used in geotechnical engineering to obtain velocity profiles (for a review, see Tokimatsu [15]).

Within the scope of the SESAME project (Site EffectS assessment using AMbient Excitation, EU-Grant No. EVG1-CT-2000-00026) both practical and theoretical aspects of single station H/V analysis as well as microtremor array analysis methods are re-evaluated in order to provide guidelines for the usage of these techniques for site effect studies. In this work we focus on the influence of instrumental layouts and ambient wavefield conditions on the applicability of different frequency wavenumber approaches and the spatial autocorrelation method for the determination of dispersion curve estimates.

TOOLS FOR AMBIENT VIBRATION ARRAY ANALYSIS

Frequency wave-number methods

We implemented several frequency wavenumber techniques in order to assess their capabilities and limitations for the use of estimating dispersion curve characteristics from ambient vibration recordings. We distinguish the following methods:

CVFK: a conventional semblance based frequency-wavenumber method after Kvaerna and Ringdahl [16] evaluated in sliding time window manner and narrow frequency bands around some center frequency. The coherence estimate is given by:

$$RP(\omega, \vec{k}) = \frac{\sum_{l=1}^L \left| \sum_{i=1}^N X_i(\omega_l) e^{i\omega_l \vec{k} \vec{r}_i} \right|^2}{\sum_{l=1}^L \sum_{i=1}^N |X_i(\omega_l) e^{i\omega_l \vec{k} \vec{r}_i}|^2} \quad \text{Eq. 1}$$

where $X_i(\omega_l)$ are the complex Fourier coefficients of the observed signals at stations i , ($i = 1, \dots, N$), at discrete frequencies ω_l , ($l = 1, \dots, L$). The phase shifts $e^{i\omega_l \vec{k} \vec{r}_i}$ account for the delay times related to the horizontal wavenumber \vec{k} from which the direction θ and the horizontal slowness s can be derived as:

$$\theta = \arctan\left(\frac{k_y}{k_x}\right) \text{ and } s = \frac{|\vec{k}|}{\omega} \quad \text{Eq. 2}$$

In order to obtain the propagation characteristics of the most coherent plane wave arrival, a grid search over the wavenumber plane is performed. For all presented f-k approaches we used here a wavenumber grid layout sampled equidistantly in slowness and azimuth (azimuthal resolution set to 5 degrees, slowness resolution set to 0.025 s/km).

- **CVFK2:** the conventional frequency wavenumber estimate is based on the evaluation of the cross spectral matrix $R(\omega) = E \langle X(\omega)X^H(\omega) \rangle$ (CSM), where $E \langle \cdot \rangle$ denotes the expectation value. The CSM is estimated by a block-averaging technique of the observed signal contributions at the array stations $X(\omega) = [X_1(\omega), \dots, X_N(\omega)]$ for a given target frequency. The conventional estimator can be written in matrix notation as:

$$P(\omega, \vec{k}) = A(\omega, \vec{k}) R A(\omega, \vec{k})^H \quad \text{Eq. 3}$$

where $A(\omega, \vec{k}) = [e^{j\vec{k}\vec{r}_1} \dots e^{j\vec{k}\vec{r}_N}]^T$ are the steering vectors for wavenumber \vec{k} at frequency ω .

- **CAPON:** the high-resolution frequency wavenumber approach after Capon [14] is based on the CSM estimate $R(\omega)$. The estimator is constructed to minimize the spectral leakage in the wavenumber domain and is then given by:

$$P(\omega, \vec{k}) = \frac{1}{A(\omega, \vec{k})^H R(\omega)^{-1} A(\omega, \vec{k})} \quad \text{Eq. 4}$$

This f-k technique is the most widely used within the context of microtremor analysis (Tokimatsu [15]).

- **MUSIC:** this high-resolution frequency wavenumber method introduced by Schmidt [17] is based on the decomposition of the cross-spectral matrix into signal and noise subspace. MUSIC is a noise subspace approach and determines estimates of the signal characteristics from:

$$P(\omega, \vec{k}) = \frac{1}{A(\omega, \vec{k})^H E_N(\omega)^H E_N(\omega) A(\omega, \vec{k})} = \frac{1}{\sum_{i=q+1}^N |A_i(\omega, \vec{k}) \vec{E}_{N_i}(\omega)|^2} \quad \text{Eq. 5}$$

$\vec{E}_{N_i}(\omega)$ are the sorted eigenvectors of the CSM $R(\omega)$ and $q(1 \leq q \leq N-1)$ is the number of eigenvectors spanning the signal subspace. The parameters of propagation of the q multiple signal arrivals are determined by the minimization of the projection on the noise subspace of the q corresponding wavenumber vectors (Eq. 5). To take full advantage of the high-resolution capabilities of the MUSIC algorithm an optimal separation of the signal and noise subspaces is required. In this study, we used a statistical approach, based on an information theory criterion (Akaike [18], Wax and Kailath [19]). Analog to the sliding window analysis scheme of the CVFK algorithm, we evaluated slowness estimates on a statistical basis (MUSIC), or estimated the CSM by block-averaging (MUSIC2). For a detailed overview of these and other f-k estimators, see Zywicki [20].

Spatial autocorrelation method (SPAC) and modification

Whereas the frequency wavenumber techniques are based on the assumption of the validity of the plane wave signal model, the spatial autocorrelation method (SPAC, Aki [10]) bases its theoretical foundation on the precondition of a stochastic wavefield which is stationary in both time and space. Aki [10] showed, that, given this assumption, the existing relation between the spectrum densities in space and time can be used to derive the following expression:

$$\bar{\rho}(r, \omega) = J_0 \left(\frac{\omega r}{c(\omega)} \right) \quad \text{Eq. 6}$$

$\bar{\rho}(r, \omega) = \int_0^\pi \rho(r, \omega, \theta) d\theta$ represents the azimuthally averaged spatial autocorrelation $\rho(r, \omega, \theta)$ for station pairs separated by distance r and the interstation direction θ , and J_0 denotes the Bessel function of the first kind and zero-th order. The above relation allows deriving the single valued phase velocity $c(\omega)$ at a given frequency ω by inversion from observed averaged spatial autocorrelation coefficients. Aki [10] suggested the use of dense semicircular array deployments to readily obtain these autocorrelation coefficients for various radii and target frequencies and applied this technique for the analysis of surface wave dispersion characteristics from microtremor recordings.

Bettig et al. [21] suggested a modification of Aki's original SPAC formula which allows applying the spatial autocorrelation method for less ideal experimental array configurations. The modification concerns the evaluation of the averaged spatial autocorrelation coefficients from station pairs taken from rings of finite thickness $r_1 \leq r \leq r_2$ instead of using a fixed radius r . The modified formula for the averaged autocorrelation coefficient is:

$$\bar{\rho}(r_1, r_2, \omega) = \frac{2}{r_2^2 - r_1^2} \int_{r_1}^{r_2} r J_0 \left(\frac{\omega r}{c(\omega)} \right) dr = \frac{2}{r_2^2 - r_1^2} \frac{c(\omega)}{\omega} \left[r J_1 \left(\frac{\omega r}{c(\omega)} \right) \right]_{r_1}^{r_2} \quad \text{Eq. 7}$$

Practically, the values for minimal and maximal radii r_1 and r_2 are determined from displaying the co-array configuration for arbitrary array geometries and selecting stations pairs with similar interstation distances and good azimuthal coverage for the computation of the averaged autocorrelation coefficients.

Determination of Dispersion Curves

For the determination of dispersion curves we employ the following schemes for the different f-k approaches. Using a sliding window analysis for the semblance based CVFK in narrow frequency bands, we determine the maximum in each slowness map and record the propagation parameters for the corresponding horizontal slowness vector. This allows for longer time series (several minutes) to evaluate the frequency dependent distribution of propagation parameters. The determination of dispersion curves from these distributions is more appropriate than computing first and second order statistical moments like mean, standard deviation or median and median deviation.

We visualize the histograms obtained from the CVFK analysis as density plots, overlaid by the median and median deviation estimates. For the methods based on the block-averaged CSM (CVFK2, CAPON, MUSIC2), we obtain a single slowness map for the whole analyzed time series. In order to obtain some uncertainty estimate for those methods we record additionally the propagation parameters of the 2% highest power estimates in the slowness maps. The distribution of these values are displayed as density maps overlaid by the maximal f-k estimates. For the determination of dispersion curves, these distributions, viewed as confidence regions, help considerably to judge the reliability of the slowness estimates.

In Fig. 1 we show two examples for the visualization of analysis results. For a repeatedly active source at fixed position with respect to the array setting, we show both the slowness-frequency curves evaluated from the CVFK and CAPON analysis (lower panels) as well as the directional estimates (upper panels). We choose to view the dispersion curves proportional to slowness instead of phase velocities, as this allows a linear relation to the measurement errors (time delays). Additional arguments for this way of displaying are given in Brown et al. [22]. The theoretical Rayleigh wave dispersion curves for fundamental and first higher modes are plotted for comparison (black curves). In addition, aliasing curves

are plotted for the minimal (red dashed), mean (black dashed) and maximal (green dashed) interstation distance within the array configuration. In this example the wavefield consists of fundamental Rayleigh waves only and deviations from the theoretical dispersion curves ($f < 0.6\text{Hz}$, $f \sim 1.1\text{Hz}$, $f > 2\text{Hz}$) can be related to sharp drops in the vertical component spectra.

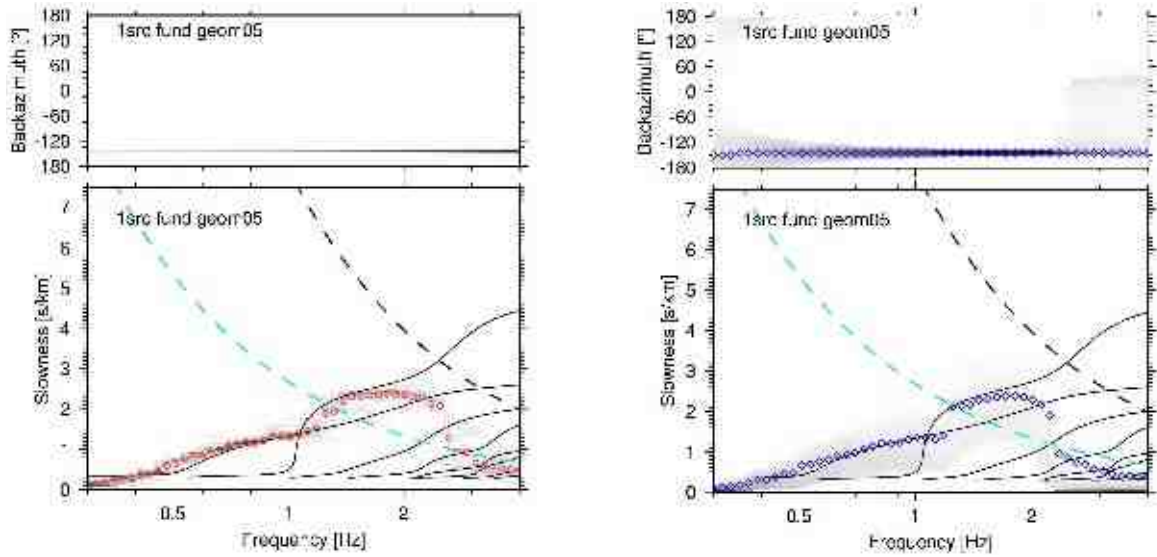


Fig. 1: Example of visualization of f-k analysis results. Left panels: semblance based sliding window CVFK analysis. Right panels: Capon estimator. Lower panels: slowness estimates (red, blue symbols), theoretical Rayleigh wave dispersion curves (black solid) and aliasing conditions (dashed lines). Underlying density plots show the distribution of estimates. Upper panels: directional estimates. The direction of the fixed source location is correctly estimated within the resolution of the employed wavenumber grid sampling (5 degree azimuthal resolution).

SIMULATING AMBIENT NOISE

In order to allow a consistent comparison of the different array techniques for estimating Rayleigh wave dispersion curves from microtremor recordings, we created several synthetic datasets simulating ambient seismic noise. The composition of ambient seismic noise wavefields is still debated in the scientific community. Different estimates for the energy ratio between body and surface waves, the ratio between Love and Rayleigh waves or the ratio between fundamental mode and higher mode surface waves contained in the ambient noise wavefield have been given. Considering the complexity of source excitation of anthropogenic activity and site specific propagation effects for distinct geologic subsurface structures, it is unlikely that a general rule can be found. Thus, as no optimal procedure for realistic ambient noise simulations can be given, we started with simplified assumptions. In particular we used point-source excitations at the earth's surface with impulsive source time functions throughout this study.

In order to account for different wavefield situations, we varied the spatio-temporal densities and force orientations. We used the modal summation technique (Hermann [23]) to compute two types of datasets:

- fundamental mode of Rayleigh waves without higher modes
- all modes of Rayleigh waves.

We considered four different cases of source configurations, starting from the simple case where only one source is acting to the case where multiple sources are randomly distributed on the medium surface. The four different cases that we considered are called '1src', '2village', 'randcart' and 'randclose' and the spatial distributions of the sources used for each of them are represented in Fig. 2. Each source is repeated several times, and the number of repetition is chosen randomly between 1 and 5 (3 in average) (see Table 1). The time of excitation, the amplitude and the force orientations that characterize each source are randomly chosen, too.

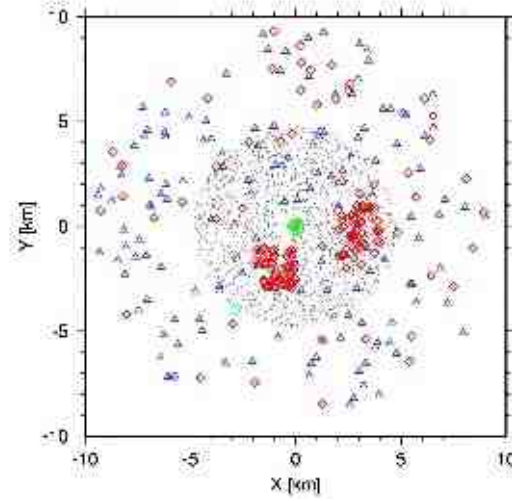


Fig. 2: Spatial distributions of the sources used to calculate the '1src' (turquoise circle), '2village' (red diamonds), 'randcart' (blue triangles) and 'randclose' (black dots) datasets. The green line represent the spiral shaped array setting.

Source configuration	Number of source locations	Number of excitations	Sources-array distances(km)	Modal summation seismograms
1src	1	50	5	16384 pts @ 50 Hz
2village	150	450	1-10	16384 pts @ 50 Hz
Randcart	150	450	1-10	16384 pts @ 50 Hz
Randclose	2000	6000	0-5	32768 pts @ 50 Hz

Table 1: Summary of source configurations

The virtual test sites

We choose two distinct 1D velocity structures as 'virtual test sites' for the simulation. Both a deeper sedimentary basin similar to the geologic situation in the Lower Rhine Embayment (NW Germany) and a very shallow site as found in the city of Liege (Belgium) have been selected for this purpose. The depth of the main impedance contrast between sedimentary layers and bedrock are found in depths of 200 m and 28 m, respectively. Fig. 3 shows the shear wave velocity depth functions and Qs attenuation structures used for the waveform modeling for the deep (left panels) and the shallow (right panels) site.

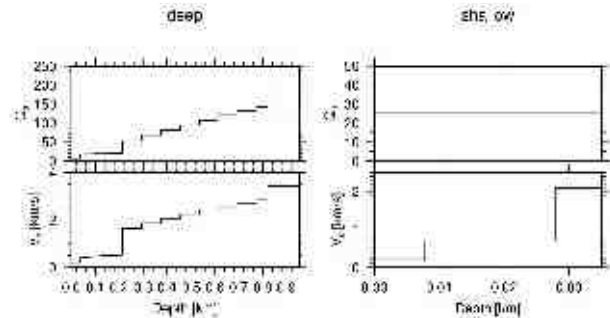


Fig. 3: Shear wave velocity depth functions (lower panels) and attenuation structures (upper panels) used for the waveform modeling for the deep (left panels) and the shallow (right panels) site.

The virtual array geometries

The noise wavefield has been calculated for a set of 50 sensors distributed along a spiral. As one of the objectives of this study was to determine the effect of the instrumental layout on the dispersion curve estimate, we choose 4 different sub-arrays, similar to realistic field experiment layouts, with variable number of sensors, shapes and apertures. The configurations are shown in Fig. 4 and are described in Table 2. In addition, the array response for the arrays with smallest and largest aperture is depicted for the frequency band 0.9 to 1.1Hz. For the smallest configuration (aperture 21m), one can recognize the low resolution capabilities from the broadness of the main peak of the array response. On contrary, for the larger configuration (aperture 557m), the resolution is improved but secondary peaks due to aliasing (insufficient sampling in the spatial domain) appear in the array response.

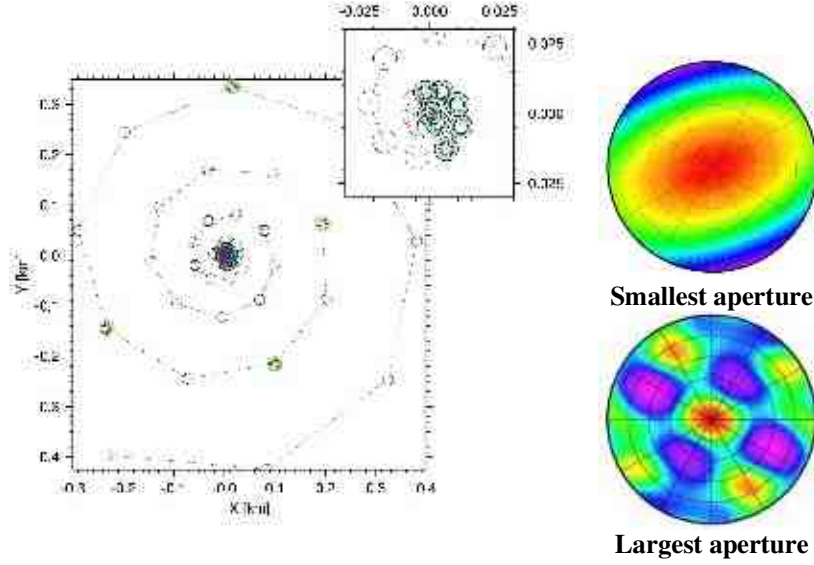


Fig. 4: The left panel represents the geometrical configuration of the 50-sensors array used for the simulations (black thin circles). We used 4 sub-arrays referred to as geom01, geom04, geom05 and geom06 in the text and represented in this figure by black, green, blue and red thick circles respectively. The top and low right panels represent the array response for the frequency band 0.9 to 1.1 Hz for the smallest (geom01) and the largest (geom04) arrays used for this study.

Name of the geometry	Number of sensors	Dmin (m)	dmean (m)	dmax (m)
geom01	7	4.4	11.4	21.5
geom04	11	4.4	184	557
geom05	11	4.4	63	187
geom06	7	7.6	272	557

Table 2: Characteristics (number of sensors, minimal, mean and maximal interstation distances) of the four sub-arrays used for this study

THE RESULTS OF F-K ANALYSIS

Influence of array geometries

We show the influence of the array geometry on the dispersion curve estimates considering two particular geometries: geom01 and geom06 (see Fig. 4, Table 2 for description). The results from the frequency wavenumber decompositions (CVFK and Capon) of the ‘randclose’ dataset (shallow site, all modes of Rayleigh waves) are presented in Fig. 5.

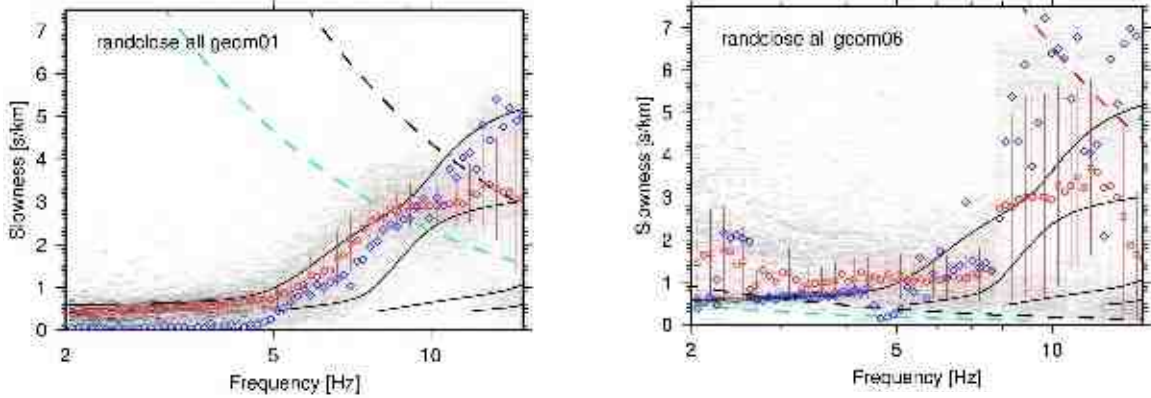


Fig. 5: Results of the CVFK and the Capon analysis for the ‘randcart’ dataset calculated for the shallow site and including all modes of surface waves (see Fig. 1 for explanation). Three different geometries have been considered: geom01 (top left panel), geom04 (top right panel) and geom06 (low left panel).

For the small aperture array (geom01), the CVFK performs relatively well in the [2Hz-9Hz] frequency band. The median values deduced from the histogram follow the theoretical dispersion curve of the fundamental mode, with slightly lower values than the one expected. This is explained by the insufficient resolution of the array at lower frequencies which is too small to separate multiple wavefield contributions coming from different directions. Even more pronounced we can observe this effect for the Capon method. In this case the bias is a result of both the insufficient wavenumber resolution and the block-averaging technique used for estimating the CSM. Between 5 and 8Hz, both methods show a simultaneous contribution for the fundamental and first higher mode which lead to intermediate values of slowness. For higher frequencies, the CVFK distribution exhibits simultaneously contribution of fundamental and higher modes as well as effects of aliasing. Less perturbation due to aliasing are observed for the Capon estimates, since the amplitude of the aliasing peaks are strongly reduced due to the construction principle of the estimator (and the block-averaging implementation of this method).

Compared to geom01, the sensor configuration of geom06 has a much larger aperture. Four of the sensors in the central part of the array are ‘re-deployed’ surrounding the three central stations in distances up to 350 m (red circles in Fig. 4). As a consequence, the CAPON estimates follow perfectly well the theoretical dispersion curve for the lower frequency part but, due to aliasing effects, no reliable estimates are obtained for frequencies higher than 5Hz. As the aperture and therefore the resolution of the array is increased for lower frequencies, the histogram obtained from the CVFK presents higher focusing around the theoretical dispersion curve in the frequency band below 4.5 Hz. At the same time, aliasing features occur at all frequencies resulting in broadly asymmetric shaped distributions. Thus, the median values and median deviations are no longer a good representation of the statistical distribution of the histograms and don’t reflect the theoretical dispersion characteristic.

Comparison between f-k methods

We compared the capability of the different frequency wavenumber decompositions (CVFK, Capon, CVFK2 and MUSIC2) to retrieve the dispersion curves for all available datasets. Exemplarily, we present the '1src' and 'randcart' source configurations for both the pure fundamental mode simulation and the dataset containing all higher mode surface waves. These datasets have been calculated for the deep sediment velocity model and the results for the station configuration geom04 are shown in **Error! Reference source not found.** for '1src' and in Fig. 7 for 'randcart'.

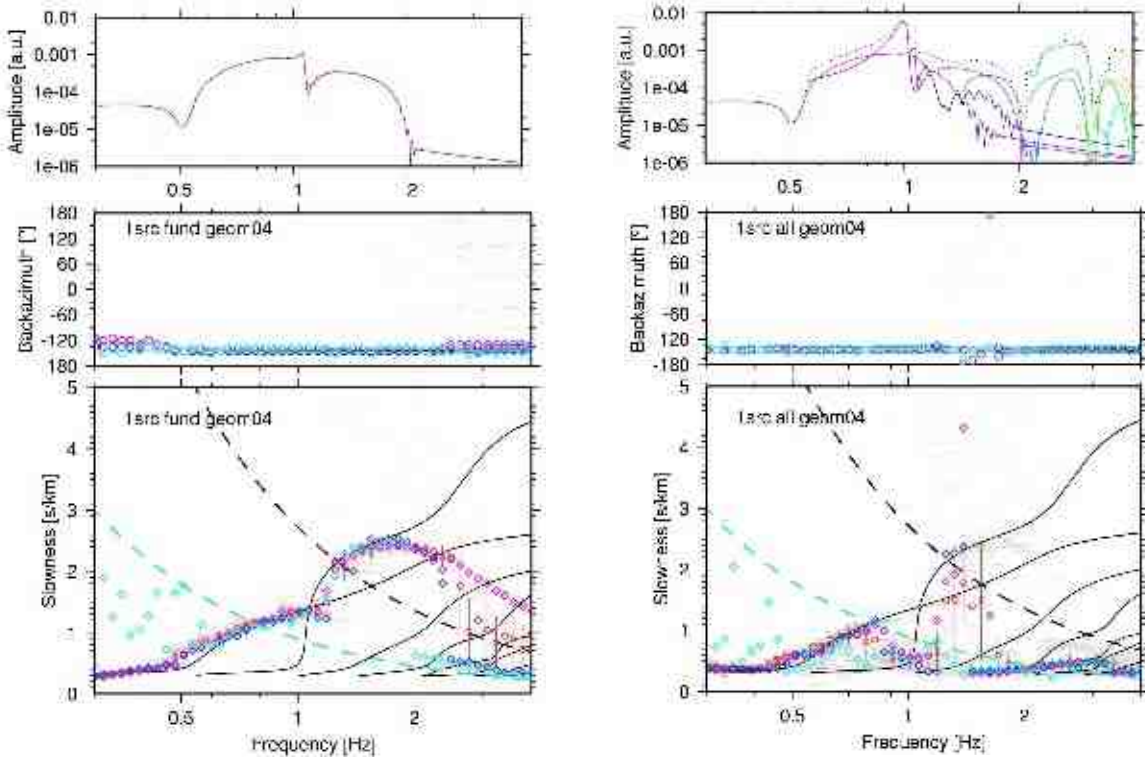


Fig. 6: Results from the frequency wavenumber decomposition using all different methods (CVFK: histogram and red dots for median values, Capon: blue diamonds, CVFK2: pink diamonds and MUSIC2: turquoise diamonds) for the '1src' source configuration including only fundamental mode (left panels) and all modes (right panels). The upper left panel represents the spectra of the fundamental mode (distance of propagation equal 5km) and the upper right panel represents the spectral contribution of the different modes (from pink to orange). The black dotted curve gives the sum of all contributions.

a) Case '1src' – fundamental mode

All methods perform well in the frequency band [0.6Hz-1.8Hz] and the frequency evolution of the slowness values follows the theoretical dispersion curve of the fundamental mode. A stable estimate of -145° is obtained for the directions of propagation which corresponds to the direction of the true source signal. Nevertheless, close to 1Hz, all methods show some scatter coinciding with the sharp drop in energy of the fundamental mode as observed in the spectra plotted in the upper left panel of **Fig. 6**. Additionally, there is a mismatch between the slowness values and the theoretical curve outside the [0.6Hz-1.8Hz] frequency band, where low spectral energy levels are observed. We think that these small deviations are associated with numerical noise in the forward calculation of the simulated wavefield which deteriorates the phase delay estimates below a certain amplitude level.

b) Case '1src' – all modes

The presence of higher modes increases considerably the complexity of the frequency-slowness distribution. In the frequency range [0.6Hz-0.8Hz], the fundamental mode is dominating and CVFK, Capon and CVFK2 give correct estimates of the slowness whereas MUSIC2 underestimates the theoretical values. In the [0.8Hz-1.8Hz] frequency band, the spectra show that 1) the first higher mode overtakes (~ 0.8 Hz), 2) there is a drop in energy of the fundamental and first higher mode and the second higher mode overtakes (~ 1.1 Hz), and 3) the fundamental mode returns to be the most energetic (~ 1.6 Hz). In this case, the bimodal distribution obtained for the CVFK describes well the simultaneous contributions of both fundamental and higher modes. However, the median values chosen to describe the statistics of the distribution are misleading. Opposed to the CVFK2 and MUSIC2 which show in this case a strong bias, CAPON gives correct estimates of the most energetic contribution (fundamental or higher) within each frequency band. For frequencies higher than 2Hz, all methods show that higher modes dominate the wavefield, and as the frequency increases, the slowness values jump from one higher mode to the next.

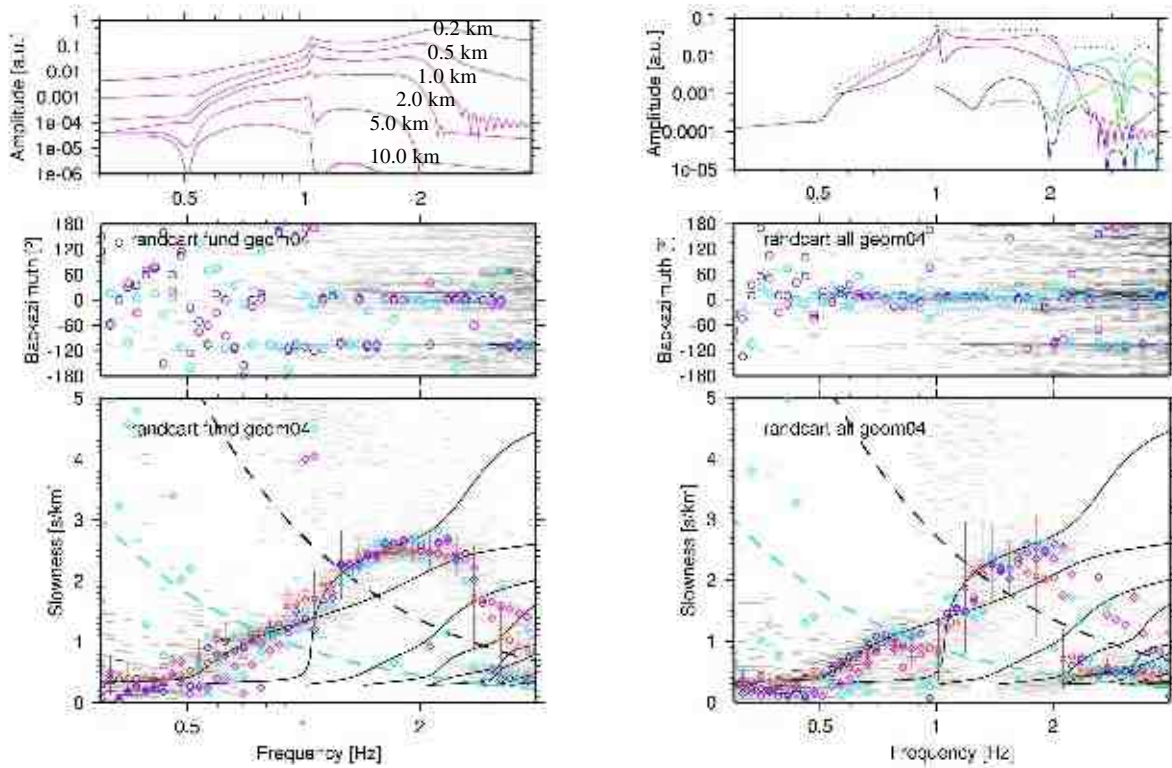


Fig. 7: Lower panels: as Fig. 6 but for the 'randcart' source configuration. The upper left panel represents the spectra of the fundamental mode for different distances of propagation (0.2, 0.5, 1, 2, 5 and 10 km) and the upper right panel represents the spectral contribution of the different modes for a 1km distance of propagation. The black dotted curve gives the sum of all contributions.

c) Case 'randcart' – fundamental mode only

The results are similar to the case '1src' but a larger scattering of the slowness values is observed around the theoretical dispersion curve for frequencies below 1Hz. We attribute this result to the simultaneous arrival of multiple plane waves from distinct directions that the array is not capable to resolve. Interferences between these multiple source contributions lead to biased slowness values, especially for the low resolution capabilities of the CVFK / CVFK2 algorithm. For frequencies above 1 Hz dominant stable source directions (0° and -120°) are estimated. This is consistent with the direction of the closest sources in the 'randcart' source configuration, lying at distances of 1 to 2 km

from the array center. The spectral levels of the fundamental mode for closer and more distant sources show larger differences for higher frequencies as can be seen from the spectra plotted on the left top panel. One possible explanation for this behavior is the relatively strong attenuation in the shallow part of the velocity model ($Q_s < 20$, Fig. 3).

d) Case ‘randcart’ – all modes

As opposed to the ‘1src’ case, the ‘randcart’ data set seems to be mainly dominated by the fundamental mode in the frequency band [0.6Hz to 2Hz]. However, around 1Hz, all methods show a decrease of the estimated slowness values. We relate this observation to the peculiar feature of our simulated source configuration. The directional estimates for frequencies above 1Hz indicate a dominant energy contribution of the closest sources between 1 and 2 km (see Fig. 2). Considering the spectra of the individual Rayleigh wave modes at 1 km distance (upper left panel of Fig. 7), the first higher mode exceeds the energy contribution of the fundamental mode around 1Hz. Above 2.2 Hz, only higher modes contribute significantly to the ambient noise wavefield. These facts are consistently reflected in the slowness frequency estimates obtained from the different f-k decomposition techniques.

COMPARISON TO MODIFIED SPAC RESULTS

We have evaluated the spatial autocorrelation coefficients for the same datasets and station configurations as used for the f-k analysis by applying the modified SPAC approach by Bettig et al. [21]. A direct comparison between the results obtained from the SPAC method and the previously discussed f-k techniques involves the inversion of observed SPAC curves into a dispersion curve. In order not to introduce additional ambiguities related to the stability of this non-linear inversion problem, we preferred to forward compute the theoretical autocorrelation curves from the theoretical dispersion curves. Therefore we can judge qualitatively the performances of the individual array methods by comparing the results against the same benchmark.

In Fig. 8 we show the frequency dependence of the averaged spatial autocorrelation coefficients for the station configuration geom05 (see Fig. 4, Table 2). From the co-array configuration we selected seven rings with mean radii ranging from 8 m to 100 m. The number of station pairs in each ring varies from 4 to 10 and the azimuth coverage spanned from 90 to nearly 180 degrees. The computation was performed for the dense random source configuration data sets (‘randclose’), both for the fundamental mode Rayleigh wave simulation (left panels) as well as for the case including all higher modes (right panels). We additionally plotted the results of the CVFK and CAPON analysis results for these datasets. We converted the slowness-frequency pairs to frequency-spatial autocorrelation pairs, using Eq. 6 for the minimal and maximal radius for each ring. The distribution of the CVFK results are shown as density plot, the CAPON results are given as individual point estimates.

By comparing the theoretical autocorrelation curves computed from the fundamental (red) and first and second higher modes (green, blue) of the Rayleigh wave dispersion curves to the measured data, we can recognize a very good agreement between the observation and theory for the fundamental mode case. It can especially be noted that for the larger rings a very good match is obtained, which nearly spans the complete frequency band. It is recognized, that both f-k measurements agree very well within the frequency band from 0.7 Hz to 2.5 Hz to the autocorrelation curves. Interestingly, the SPAC outperforms the f-k methods for higher frequencies, following nicely the theoretical dispersion relation, whereas the f-k estimates scatter significantly and don’t show any clear relation to the theoretical curve.

A similar good fit between the f-k results and the theoretical and observed autocorrelation curves is obtained for the data set including all higher modes below the frequency limit of 2 Hz. However, above this limit, the observed AC-curves show a clear deviation from the theoretical AC-curves and also the f-k analysis results do not show a clear fit to any of the individual modal autocorrelation curves. We attribute this behavior to the dominating energy contribution of higher modes (compare Fig. 7). A simple

interpretation can not be given in this case, and advanced inversion strategies including higher mode contributions must be used, which requires additional assumptions about the energy partitioning between the individual modes contributing to the mixed wavefield.

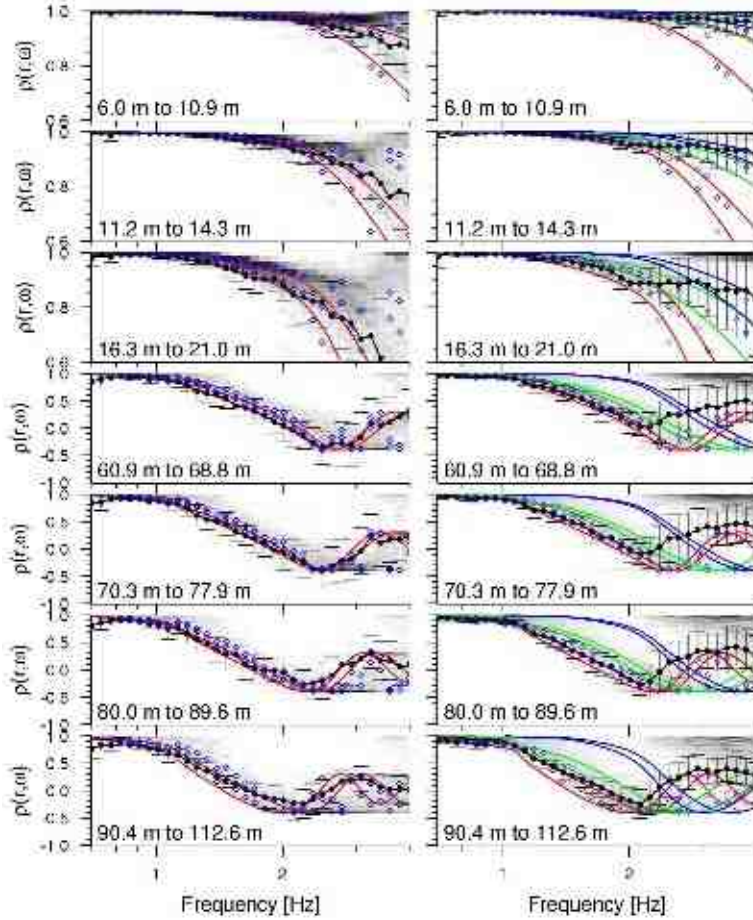


Fig. 8: Averaged spatial autocorrelation coefficients evaluated for 50 frequencies between 0.3 Hz and 4.0 Hz (black dots). From top to bottom, the ring dimension increases from ca. 8 m to 100 m. On the left, we evaluated the simulated fundamental mode Rayleigh wave data set, using the source configuration ‘randclose’. Overlaid are the theoretical autocorrelation curves computed from the fundamental mode dispersion curve for the given velocity model and radii r_1 and r_2 (red curves). On the right we used the same source configuration, but including all higher modes. The theoretical autocorrelation curves for the fundamental and first two higher modes are overlaid (red green blue). For the interpretation, see text.

DISCUSSION AND CONCLUSION

We compared the performance of different frequency wavenumber approaches as well as the spatial autocorrelation method in order to determine under which circumstances high-quality site-specific surface wave dispersion characteristics can be obtained from the analysis of microtremor wavefields. Using simulated ambient vibration wavefields, we studied the influence of both the array layout (number of sensors, geometry and interstation distances) and source characteristics as well as propagation effects of the noise wavefield for each of the employed methods.

For the simplest case, one dominant source and fundamental mode only, we found that all methods perform equivalently well. Considering more realistic wavefield situations, randomly distributed sources and/or higher mode contributions, the direct interpretation of frequency-slowness values becomes more difficult. In particular we observed significant bias of slowness values in case of insufficient resolution capabilities of the array configurations. In addition, in case that higher mode Rayleigh waves contribute significantly to the total energy, mixed dispersion curve characteristics will be obtained. For well resolving configurations it is, for favorable wavefield situations, possible to separate individual mode contributions. However, the interpretation of which mode is observed is not straight forward. For the inversion of shear velocity profiles advanced strategies have to be employed to make use of this information.

For the practical task of dispersion curve determination from ambient vibration array recordings we suggest the use of combinations of various f-k methods. As most stable algorithm we regard the conventional f-k (CVFK). Although it offers only low resolution capabilities, it allows to determine robust propagation characteristic distributions when applied in a sliding window analysis. We find that these distributions are especially advantageous for the visualization and determination of reasonable uncertainty measures to recognize the validity of dispersion curve estimates. Capon's high resolution f-k approach (CAPON) is well suited to complement the CVFK analysis, as it gives less biased estimates and allows phase velocity determination for higher frequencies where aliasing is already deteriorating the CVFK results. In addition to CVFK and CAPON frequency-wavenumber decompositions, we suggest to use the spatial autocorrelation method in order to further cross-check the results on the same array data set. Compared to frequency-wavenumber methods, the SPAC gives reliable estimates of the dispersion characteristics within a larger frequency band, and allows additionally an easier recognition of the presence of higher modes from the unexpected occurrence of oscillations in the autocorrelation curves. Less suitable for the goal of dispersion curve estimation are the CVFK2 and MUSIC2 approaches. CVFK2 exhibits a limited resolution capability whereas the main drawback of the MUSIC2 algorithm is the difficulty to reliably assess the number of sources spanning the signal subspace for the typical multi-source situations in the ambient vibration wavefield.

From the tests performed we conclude the following for the interpretation of dispersion curves: the valid frequency band for interpreting the dispersion characteristics obtained from f-k analysis techniques is limited on both sides. For low frequencies the limitation is either caused by insufficient resolving capabilities of the chosen array layout or by the vanishing spectral energy contribution of the vertical Rayleigh wave displacements (for example related to the degenerated horizontal ellipticities around the frequency of the H/V spectral peak location). The upper limit is given by the occurrence of aliasing patterns due to insufficient spatial sampling of the wavefield. In order to improve the determination of dispersion curves, we recommend the use of adaptive array deployment strategies. Array apertures and interstation distances should be adapted for distinct target wavelength ranges. Thus, starting from short wavelengths and going to higher wavelengths well resolved partial dispersion curves can be obtained even in complex wavefield situations. However, ambient noise excitation as well as particular propagation effects may lead to misinterpretation of phase velocities or autocorrelation coefficients obtained from array analysis. The use of various combinations of analysis methods may allow to prevent this eventual misinterpretation by providing complementary information on the ambient vibration wavefield characteristics. Contradictory results obtained from the individual methods may be an indicator to recognize such situations.

ACKNOWLEDGEMENTS

We thank the members of the SESAME group for helpful discussions, comments and suggestions. All maps and figures were generated with the Generic Mapping Tools GMT (Wessel and Smith, 1991). M. Ohrnberger has been financed by EU-Grant No. EVG1-CT-2000-00026 (SESAME). E. Schissle has been funded by IQN Potsdam (DAAD).

REFERENCES

1. Borchardt R.D. "Effects of local geological conditions in the San Francisco Bay region on ground motions and the intensities of the 1906 earthquake". Bull. Seism. Soc. Am. 1970: 60, 29-61.
2. Campbell K.W. "A note on the distribution of earthquake damage in Long Beach, 1933". Bull. Seism. Soc. Am. 1976: 66, 1001-1006.
3. Hartzell S., Leeds A., Frankel A., and Michael J. "Site response for urban Los Angeles using aftershocks of the Northridge earthquake". Bull. Seism. Soc. Am. 1996: 86(1B), S168-S192.
4. Yamanaka H. "Geophysical explorations of sedimentary structures and their characterization". Irikura K., Kudo K., Okada H., and Sataini T., Editors. The Effects of Surface Geology on Seismic Motion, Rotterdam, Balkema, 15-33, 1998.
5. Horike M. "Inversion of phase velocity of long-period microtremors to the S-wave-velocity structure down to the basement in urbanized area". J. Phys. Earth 1985: 33, 59-96.
6. Ishida H., Nozawa T. and Niwa M. "Estimation of deep surface structure based on phase velocities and spectral ratios of long-period microtremors". Irikura K., Kudo K., Okada H., and Sataini T., Editors. Effects of Surface Geology on Seismic Motion, Yokohama, Rotterdam, Balkema, 697-704, 1998.
7. Miyakoshi K., Kagawa T. and Konioshita S. "Estimation of geological structures under the Kobe area using the array recordings of microtremors". Irikura K., Kudo K., Okada H., and Sataini T., Editors. The Effects of Surface Geology on Seismic Motion, Rotterdam, Balkema, 691-696, 1998.
8. Yamanaka H., Takemura M., Ishida H., and Niwa M. "Characteristics of long-period microtremors and their applicability in exploration of deep sedimentary layers", Bull. Seism. Soc. Am. 1994: 84(6), 1831-1841.
9. Scherbaum F., Hinzen K.-G., and Ohrnberger M. "Determination of shallow shear wave velocity profiles in the Cologne, Germany area using ambient vibrations". Geophys. J. Int. 2003: 152, 597-612.
10. Aki K. "Space and time spectra of stationary stochastic waves, with special reference to microtremors", Bull. Earthquake Res. Inst. Tokyo Univ. 1957: 35, 415-456.
11. Lacoss R.T., Kelly E.J., and Toksoez, M.N. "Estimation of seismic noise structure using arrays". Geophysics 1969: 34, 21-38.
12. Horike M., "Geophysical exploration using microtremor measurements". Xth WCEE, Acapulco, 1996: Paper no. 2033, Elsevier Science Ltd.
13. Matsushima T. and Okada H. "Determination of deep geological structures under urban areas using long-period microtremors", BUTSURI-TANSA 1990: 43(1), 21-33.
14. Capon J. "High-resolution frequency-wavenumber spectrum analysis". Proc. IEEE 1969: 57, 1408-1418.
15. Tokimatsu K. "Geotechnical site characterization using surface waves", Ishihara, Editor. Earthquake Geotechnical Engineering, Rotterdam, Balkema, 1333-1368, 1997.
16. Kvaerna T. and Ringdahl F. "Stability of various f-k estimation techniques". Semiannual technical summary, 1 October 1985 – 31 March 1986, NORSAR Scientific Report, 1-86/87, Kjeller, Norway, 29-40, 1986.
17. Schmidt, R.O. "Multiple source DF signal processing: an experimental system". IEEE Trans. Ant. Prop. 1986: AP-34(3), 281-290.
18. Akaike, H. "Information theory and an extension of the maximum likelihood principle". Proc. 2nd Int. Symp. Inform. Theory, 1973: 267-281.
19. Wax M. and Kailath, T. "Detection of signals by information theoretic criteria". IEEE Transactions on ASSP, 1985: 33(2), 387-392.
20. Zywicki D. J. "Advanced signal processing methods applied to engineering analysis of surface waves", PhD. Thesis Georgia institute of technology, 227 p., 1999.

21. Betti B., Bard P.-Y., Scherbaum F., Riepl J., and Cotton F. "Analysis of dense array noise measurements using the modified spatial auto-correlation method (SPAC). Application to the Grenoble area". *Bolletino di Geofisica Teorica ed Applicata* 2003: 42(3/4), 281-304.
22. Brown L.T., Boore D.M., and Stokoe II K.H. "Comparison of Shear-Wave Profiles at 10 Strong-Motion Sites from Noninvasive SASW Measurements and Measurements Made in Boreholes". *Bull. Seism. Soc. Am.*, 2002: 92(8), 3116-3133.
23. Hermann R.B. "Computer programs in seismology, Version 3.0", 1996.